Climate Dynamics (2003) 21: 539–557
DOI 10.1007/s00382-003-0351-3

C. S. Jackson · A. J. Broccoli

Orbital forcing of Arctic climate: mechanisms of climate response and implications for continental glaciation

Received: 9 July 2002 / Accepted: 10 July 2003 / Published online: 4 November 2003

Abstract Progress in understanding how terrestrial ice volume is linked to Earth's orbital configuration has been impeded by the cost of simulating climate system processes relevant to glaciation over orbital time scales (10^3–10^5 years). A compromise is usually made to represent the climate system by models that are averaged over one or more spatial dimensions or by three-dimensional models that are limited to simulating particular "snapshots" in time. We take advantage of the short equilibration time ($\backsim$10 years) of a climate model consisting of a three-dimensional atmosphere coupled to a simple slab ocean to derive the equilibrium climate response to accelerated variations in Earth's orbital configuration over the past 165,000 years. Prominent decreases in ice melt and increases in snowfall are simulated during three time intervals near 26, 73, and 117 thousand years ago (ka) when aphelion was in late spring and obliquity was low. There were also significant decreases in ice melt and increases in snowfall near 97 and 142 ka when eccentricity was relatively large, aphelion was in late spring, and obliquity was high or near its long term mean. These "glaciation-friendly" time intervals correspond to prominent and secondary phases of terrestrial ice growth seen within the marine δ^{18}O record. Both dynamical and thermal effects contribute to the increases in snowfall during these periods, through increases in storm activity and the fraction of precipitation falling as snow. The majority of the mid- to high latitude response to orbital forcing is organized by the properties of sea ice, through its influence on radiative feedbacks that nearly double the size of the orbital forcing as well as its influence on the seasonal evolution of the latitudinal temperature gradient.

C. S. Jackson (✉)
Program in Atmospheric and Oceanic Sciences,
Princeton University,
Princeton, NJ 08542, USA
E-mail: charles@ig.utexas.edu

A. J. Broccoli
NOAA/Geophysical Fluid Dynamics Laboratory,
Princeton, NJ 08542, USA

Present address: C. S. Jackson
Institute for Geophysics,
The John A. and Katherine G. Jackson School of Geosciences,
The University of Texas at Austin, 4412 Spicewood Springs Rd.,
Bldg 600, Austin, TX 78759, USA

Present address: A. J. Broccoli
Department of Environmental Sciences,
Rutgers University, New Brunswick,
NJ 08903 USA

1 Introduction

The growth and decay of terrestrial ice sheets during the Quaternary ultimately result from the effects of changes in Earth's orbital geometry on climate system processes. This link is convincingly established by Hays et al. (1976) who find a correlation between variations of terrestrial ice volume and variations in Earth's orbital eccentricity, obliquity, and longitude of the perihelion. One of the earliest and most widely known hypotheses concerning the effects of orbital configuration on glacial cycles is described by Milankovitch (1941), who presents an argument that a decrease in summer insolation is critical for glacial initiation. The usual interpretation of the Milankovitch hypothesis is that a reduction in summer insolation directly affects the amount of ice melt that occurs during that season to a point when snow fields can build upon previous year's accumulation. In this usual interpretation, the Milankovitch hypothesis is centered on the effects of orbital configuration on snow melt (or ablation) rates.

Other hypotheses have been presented as well. Young and Bradley (1984) argue that the meridional insolation gradient is a critical factor for the growth and decay of terrestrial ice through its control over poleward moisture transports and snowfall. Ruddiman and McIntyre (1981), Miller and deVernal (1992), and Imbrie et al.

(1992) suggest the North Atlantic Ocean circulation is important for modulating ice volume. Ruddiman and McIntyre (1981) and Miller and deVernal (1992) found evidence within the geologic record that the North Atlantic remains warm during periods of ice growth and conjecture that enhanced meridional temperature gradients and evaporation rates during winter enhance the delivery of snow to the nascent ice sheets of northeastern Canada. Imbrie et al. (1992) propose that orbital forcing affects North Atlantic deep-water formation and, through a chain of causality involving the Southern Ocean, atmospheric CO_2 levels.

Three-dimensional climate models provide opportunities to explore some of these hypotheses within a physically consistent framework. Unfortunately, the large computational cost of simulating more than a century or two with the most comprehensive climate models imposes an important constraint on modeling glacial-interglacial cycles. This constraint has focused research efforts towards more feasible targets, such as identifying the necessary factors that allow glaciation to occur at the inception of the most recent glacial cycle at approximately 115 thousand years before present (ka).

The 115 ka time period is of interest not only because it corresponds to a time of early growth of land ice, but also because the distribution of land ice and atmospheric concentration of CO_2 were similar to present. The main boundary condition that may account for differences between present and 115 ka is the difference in orbital configuration. A number of modeling studies have attempted to simulate glacial inception by prescribing the 115 ka orbital geometry in climate models consisting of an atmospheric general circulation model (AGCM) coupled to a simple slab ocean (Rind et al. 1989; Oglesby 1990; Mitchell 1993; Phillipps and Held 1994; Dong and Valdes 1995; Gallimore and Kutzbach 1995). These modeling studies discuss the importance of feedbacks involving sea ice and soil moisture. Sea-ice feedbacks play a role in amplifying the annual mean cooling as well as shaping seasonal response to changes in insolation. Moreover, sea-ice dynamics serve as a negative feedback on sea ice thickness, positive feedback on sea ice concentration, and a positive feedback on surface air temperature for an orbital configuration at 115 ka (Vavrus 1999). Increases in soil moisture in the mid- to high latitudes are also noted in several studies and could be playing a significant role in maintaining cooler surface air temperatures as well as increasing precipitation over land at 115 ka (Mitchell 1993; Phillipps and Held 1994). An increase in storm activity, which leads to increased precipitation rates in simulations of orbital forcing at 115 ka, is found by Kageyama et al. (1999) in an AGCM with specified sea surface temperatures (SSTs). The change in storm activity is directly related to increases in the meridional temperature gradient forced by a wintertime warming of the continents consistent with the change in radiative forcing.

A common feature of many of these studies of glacial initiation is an inability to maintain year-round snow cover from orbital forcing alone. The prescription of at least an initial meter of snow over land points north of 45°N is also insufficient to create conditions favorable for glacial initiation in several experiments (Oglesby 1990; Rind et al. 1989; Phillipps and Held 1994). In contrast to other experiments, the model employed by Dong and Valdes (1995) is sufficiently sensitive to radiative changes at 115 ka to reach the critical threshold of summer cooling noted by Rind et al. (1989) that allowed the annual accumulation of snow over many grid cells of the high Arctic, although not necessarily where the geologic record suggests glacial initiation took place. One reason some climate models may lack the necessary sensitivity is due to a warm bias in summer surface air temperatures within the northern high latitudes, a common feature in many model predictions of modern climate (Vettoretti and Peltier 2003a, b). The reduction of this bias leads to an enhanced sensitivity and permanent snow cover over part of the northern high latitudes in response to insolation anomalies at 115 ka.

The failure of many climate models to simulate permanent snow cover over Eurasia and North America at 115 ka could indicate that those models have neglected a critical feedback. Vegetation feedback is one possible candidate. Cooler summers were found to be a factor in forcing a conversion of high-latitude taiga and deciduous forests to higher albedo tundra, a process that contributed to glacial initiation in the modeling studies of de Noblet et al. (1996) and Gallimore and Kutzbach (1996). Recently, the coupled, three-dimensional, atmosphere-ocean modeling study of Khodri et al. (2001) found the amplifying effects of orbital forcing on the North Atlantic sea surface temperatures to be critical to glacial initiation, through reductions in the strength of the thermohaline circulation in addition to increased poleward moisture transports within the atmosphere. For a variety of reasons, which we will discuss in more detail toward the end of this study, the importance of these feedbacks in the real climate system remains uncertain.

While identifying the necessary factors that led to glacial initiation at 115 ka is important to quantifying some aspects of orbital forcing of glacial cycles, we also need to identify processes that are important to the evolution of terrestrial ice volume that may or may not be the same as those processes emphasized from studies of climate at 115 ka. Time series analysis of oceanic sediments reveals that ice volume has varied linearly with obliquity and precessional forcing since at least 800 ka (Imbrie et al. 1984). This suggests that orbital forcing has affected climate in a systematic fashion, and that knowledge gained from examining time slices other than 115 ka would be relevant to identifying processes that link orbital configuration with glacial-interglacial cycles. In fact, the most direct way to identify such processes is to directly model the temporal evolution of climate over orbital time scales. Because the computational demands of three-dimensional climate models are beyond our present computing power, at least in a

practical sense, other modeling strategies have been developed.

A common approach to modeling time-dependent climate response on orbital time scales is to use reduced-order models that average over one or more spatial dimensions. Examples of such models are energy balance models (EBMs), coupled EBM-ice sheet models, or other reduced dimension models (Suarez and Held 1979; Schneider and Thompson 1979; Held 1982; Deblonde and Peltier 1991, 1993; Short et al. 1991; Gallee et al. 1992; Marisiat 1994; Ledley and Chu 1995; Peltier and Marshall 1995; Tarasov and Peltier 1997). These models have performed remarkably well to describe the radiative effects of insolation and CO_2 on surface air temperature and are able to reproduce terrestrial ice volume changes on precession, obliquity, and even eccentricity time scales. Although many of these models contain some parameterization of the hydrologic cycle, variations in ablation rates dominate modeled changes in ice volume (Tarasov and Peltier 1997). A question still remains, however, as to why lower-order models can initiate glaciation at 115 ka solely from orbital forcing when many more complete climate system models cannot.

An alternate strategy for generating time series of model predictions over orbital time scales without compromising the ability to resolve the dynamics of the atmosphere is to string together a series of snapshot equilibrium experiments through a time interval of interest. Such an approach is taken in a series of experiments of deglaciation in which reconstructions of orbital configuration, CO_2 concentrations, and terrestrial ice sheets were used to force a climate model consisting of an atmospheric GCM coupled to a slab ocean at 3 ky intervals between 18 ka and present (Kutzbach and Guetter 1986; Kutzbach 1987; Felzer et al. 1998). A slightly different approach was adopted by Prell and Kutzbach (1987) in their study of the effect of orbital forcing on time series records of monsoon strength over the last 150 ky. Through a series of equilibrium experiments meant to determine the separate influence of eccentricity scaled precession, obliquity, and ice-sheet extent on monsoon strength, they derived a linear prediction of the time series of monsoon strength that scaled with the known variations in orbital configuration and ice volume.

In this study, we explore the time-dependent response of Arctic climate to orbital forcing over the past 165,000 years by combining the strengths of a three-dimensional climate model with the time series approach typically reserved for lower-order models. We accomplish this by using a computationally efficient climate model, consisting of an atmospheric GCM coupled to a simple mixed layer ocean, and accelerating the orbital forcing such that the integration is practicable with existing computer resources. Our choice of a GCM (rather than a lower-order model) is dictated by our interest in processes affecting precipitation, such as cyclone dynamics and moisture transports. In this approach, we are deliberately neglecting a number of potentially important feedbacks, including ocean dynamics, atmospheric composition, glacier dynamics, and vegetation. This simplified experimental design allows us to better understand processes involving the atmosphere and its interactions with the land surface, sea ice, and the oceanic mixed layer. We focus our analysis on the response of Arctic climate and mechanisms that affect it, particularly those processes that are relevant to continental glaciation.

2 Model design

The climate model used in the orbital forcing experiments is nearly identical to the one used by Broccoli (2000) to simulate the ice age climate, differing only in the choice of resolution. The model consists of an atmospheric GCM, land surface model, and a static mixed-layer ocean model, which includes a dynamic-thermodynamic model of sea ice. Earlier versions of this model have been used to examine the climate response to changes in boundary conditions at the Last Glacial Maximum (Manabe and Broccoli 1985; Broccoli and Manabe 1987). We shall include here a brief description of the various components of the climate model that are used in the orbital forcing experiment.

The atmospheric component numerically solves the primitive equations using the spectral transform technique. We have chosen to use a coarsely resolved atmosphere with 9 unevenly spaced levels in the vertical, and R15 spectral transform truncation with equivalent grid spacing of approximately 4.5° latitude by 7.5° longitude. The choice of this lower resolution is dictated by the need to minimize the computational expense of the experiment, which will be elaborated in the following section.

The land-surface model determines surface temperature in a heat balance calculation that is constrained by the requirement that no heat is stored within the surface. Soil moisture is predicted through a simple 'bucket' formulation in which the soil has a holding capacity of 15 cm depth of water. Any water accumulation in excess of 15 cm depth is assumed to be runoff. Snow cover is also predicted based on snowfall, sublimation, and snowmelt, but has no limits to its accumulation. Since there is no storage of heat within the surface, over snow covered surfaces excess surface energy will go toward melting of snow via the latent heat of melting of ice to water. There is no account concerning refreezing of surface melt. Because the model does not include any formulation for glacier dynamics, the model will not allow land ice to expand into neighboring grid cells through ice deformation.

The mixed-layer ocean consists of a static, isothermal slab of 50 m depth, which is sufficient to account for the seasonal storage of heat within the upper ocean. An additional source or sink of heat is prescribed within the model mixed layer, varying with location and season, and is intended to mimic the transport of heat by ocean currents. These heat flux adjustments are determined within a simulation of modern day climate in which observed SSTs and sea ice are prescribed, and they equal the amount of heat that is needed to maintain the observed SST and sea-ice distribution. When the model is appropriately tuned to give radiative balance at the top-of-the-atmosphere, the global mean heat flux adjustments will be near zero. When fully tuned, the model was able to achieve a radiative balance to within 1.2 W m^{-2}, which we consider acceptable for a model of this kind.

Some smoothing of the calculated heat flux adjustments is employed in the southern extratropics. For latitudes south of 40°S, the applied flux adjustments are replaced by the zonal mean of the calculated values. In the belt from 30°S to 40°S, the applied flux adjustments are a weighted average of the zonal mean and calculated values, with the weighting varying linearly over that latitude range. This smoothing is needed to avoid excessive sea-ice growth when sea ice extends over points with negative annual mean heat flux adjustments. Negative flux adjustments occur because the storm track is too weak in the R15 AGCM, leading to

insufficient cloudiness and an excess of solar radiation received at the surface.

Sea-ice dynamics and thermodynamics are simulated according to the formulation of Flato and Hibler (1992). Their formulation is based on the physics of cavitating fluids as a means to predict the formation of leads, which are important to a more realistic representation of the exchange of energy between the mixed-layer ocean and the atmosphere.

3 Experimental design

The objective of this modeling experiment is to simulate the equilibrium climate response to the continually varying orbital configuration of the Earth over the past 165,000 years. We have reduced the computational cost by accelerating the variations in orbital configuration by a factor of 30, so that the actual length of the integration is reduced to 5500 years. This amount of acceleration can be justified by the relatively short response time of the atmosphere/mixed-layer ocean system to a given change in external forcing, which is on the order of 10 years, or more than 3 orders of magnitude faster than the highest frequency component of orbital forcing. A more strict constraint on the choice of acceleration factor is dictated by the need to discern the climatic response of the climate system model to changes in orbital configuration through the noise of the model's internal variability. A model integration of 30 years is usually sufficient for this purpose. Therefore, by accelerating the variations in orbital configuration by a factor of 30, one should be able to discern the climatic effects of 1 ky increments in orbital evolution. Because we have selected a model that adjusts rapidly and will always be in near-equilibrium with the prescribed changes in orbital configuration, we have chosen to apply the variations in orbital configuration backwards in time. This provides the flexibility to extend the integration further back in time beyond 165 ka as resources allow.

The variations in Earth's orbital configuration were taken from the work of Berger (1992) (Fig. 1) and involve three parameters: eccentricity, obliquity, and the longitude of perihelion. These parameters are updated monthly during the model integration. Each year of the model is defined to have 365 days and fixes the vernal equinox on March 21st in accordance with the Paleoclimate Model Intercomparison Project (Joussaume and Taylor 1995). Because the rate of change of the seasons depends on the longitude of the perihelion, seasonal information may be distorted by a "calendar effect" (Joussaume and Bracconot 1997). This effect does not exist for annual mean quantities, but may complicate the interpretation of time series of seasonal or monthly means. We show monthly means without adjusting for the calendar effect. In all cases in which we use monthly means to draw important conclusions, we have confirmed that those conclusions are not sensitive to the calendar effect.

It is important to note that the variations in orbital configuration are the only boundary conditions that are allowed to vary through the model integration. There are no prescribed changes to model topography, atmospheric composition, vegetation, the size and extent of terrestrial ice sheets, or the land-sea distribution. All of these quantities are prescribed in accordance with modern values, with discretization as appropriate for the resolution of the model. Topography has been smoothed using the procedure developed by Lindberg and Broccoli (1996). While all of the aforementioned quantities have varied during the past 165,000 years, the orbital forcing experiment is designed to isolate the effect of changes in orbital configuration on climate, independent from changes in these other quantities.

Our experimental strategy to model the time evolving equilibrium climate response to orbital forcing over long time scales is similar in concept to the strategy developed by Kutzbach and Guetter (1986), except that we have chosen to make a single integration with smoothly varying forcing rather than create a time series from a number of separate equilibrium climate model integrations through a time interval of interest. By forcing a climate system model with continuous changes in orbital forcing, we make no assumption concerning the importance of any particular orbital configuration. The experimental design of Prell and Kutzbach (1987), for instance, makes the assumption that summer insolation is the critical season in which changes in orbital forcing affect the strength of the African and Asian monsoons. While this assumption is appropriate for their processes of interest, no such simplification is appropriate for the many diverse processes that can affect Arctic climate.

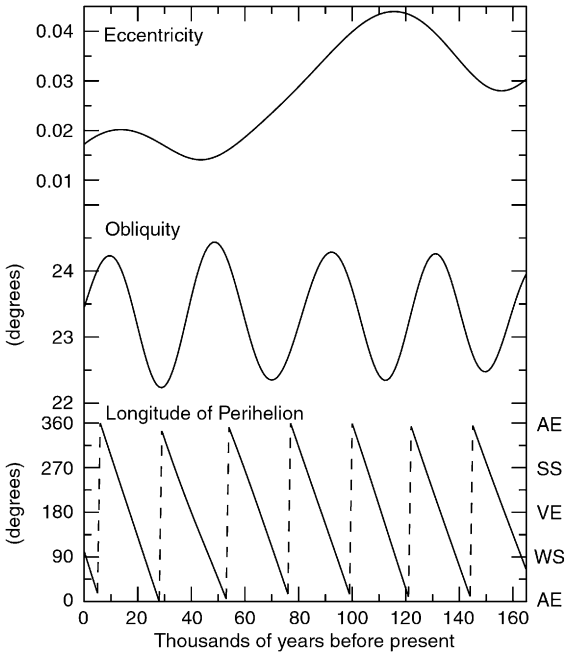

Fig. 1 The history of three parameters that specify Earth's orbital configuration over the last 165,000 years (Berger 1992). The parameters are eccentricity as the degree of non-circularity of an orbit, obliquity as the tilt of the rotation axis with respect to a line perpendicular to the orbital plane, and the longitude of perihelion as the point (or date) at which a body in orbit around the sun is at its closest approach to the Sun. The longitude of the perihelion is defined to be at 0° longitude during the Northern Hemisphere's autumnal equinox (*AE*). The remaining symbols are *WS* for the winter solstice, *VE* for the vernal equinox, and *SS* for the summer solstice

The choice to accelerate the forcing rather than to string together a number of slightly different climate simulations is mainly for the ease of model execution and the organization of model output. There is also the advantage of being able to apply time series analysis methods to the model results in a manner that might not be possible from a more choppy sequence of separate model integrations. One of the primary advantages of simulating climatic time series is to facilitate the more direct comparison between model output with climate proxy records, which are often displayed as time series. An additional advantage to generating time series simulations over orbital time scales is the prospect of using regression analysis to extract the relative importance of variations in obliquity and precession for a given climatic response.

4 Processes affecting surface air temperature

We begin our analysis by considering the variations in seasonal and annual mean surface air temperature (SAT). The imposed variations in orbital parameters induce changes in annual mean surface air temperature (Fig. 2) over northern high latitudes (60–90°N) with a

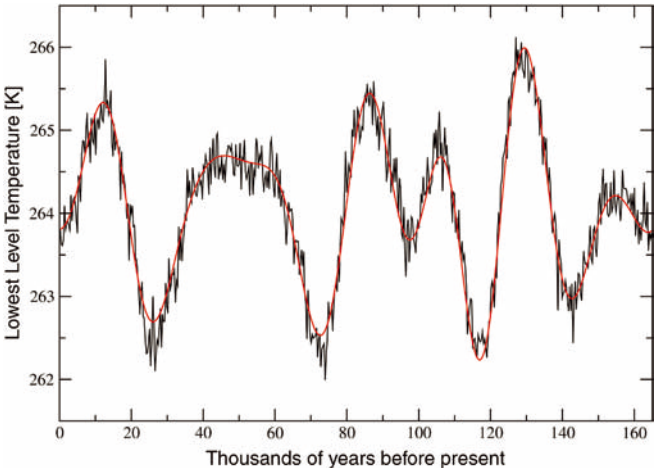

Fig. 2 Time series of annual mean surface (lowest level) air temperature averaged between 60°N–90°N. *Each point* represents a 10-year mean from the model integration. The *red curve* represents the best linear fit between obliquity and precessional variations and the time series

dynamic range of ∽4 K. Minima in annual mean SAT at 26, 73, and 117 ka indicate that these times are potentially favorable for glaciation, assuming that summer melt is minimized when annual mean SAT is low. The influences of the 41,000-year obliquity cycle and the ∽20,000-year precession cycle are evident within the annual mean SAT time series.

To quantify the contribution of obliquity and precession to variations in SAT (or any other quantity), a least squares fitting procedure is used. The time series of deviations of a given climatic quantity from its mean value over the 165,000-year simulation, $X(t)$, is expressed as:

$$X(t) = A_o\Phi'(t) + A_p e(t)\cos[\lambda(t) - \phi_p] + R(t) \quad , \qquad (1)$$

where t is time, Φ' is the deviation of obliquity from its 165,000-year mean, e is eccentricity, λ is the longitude of the perihelion. The fitting procedure determines $\mathbf{A}_o$, the amplitude of the response to obliquity, and $\mathbf{A}_p$ and ϕ_p, the amplitude and phase angle of the response to precession. The precessional forcing term ($\mathbf{A}_p e(t)\cos[\lambda(t) - \phi_p]$), equivalent to the "precession index" of Berger (1978), includes eccentricity because it modulates the effects of precession on insolation. The residual $R(t)$ contains climatic noise, nonlinear interactions between the orbital components, and any direct influence of the 100,000 year long term variations in eccentricity. To display the sensitivities of a particular quantity X to obliquity and precessional forcing, we plot $-\mathbf{A}_o$, which is the departure of X from its long-term mean for a 1-degree reduction in obliquity, and $\mathbf{A}_p e\ (t)\cos[\lambda(t) - \phi_p]$, which is the departure of X from its long-term mean for a chosen longitude of the perihelion $\lambda(t)$ and an assumed eccentricity value $e(t)$ of 0.01.

When referring to the precessional component of a given time series, we specify either the perihelion date or the aphelion date, depending on our interpretation of the season in which the solar forcing is most relevant to the quantity in question. Because the date of perihelion is always separated from the date of aphelion by six months, an orbital configuration with a late spring aphelion is identical to one with a late fall perihelion, making the choice of reference arbitrary. For non-thermal quantities where it may not be clear whether a maximum or minimum solar forcing is important (such as for storm activity) we arbitrarily choose either the aphelion or perihelion date as a reference.

Based on the least-squares fit, obliquity variations account for 51% of the temporal variance in annual mean SAT, with cold conditions associated with low obliquity. This is consistent with the insolation forcing, since low obliquity leads to decreased high-latitude insolation. Precession accounts for 43% of the variance, with coldest conditions occurring when aphelion occurs on May 20th. (Note that this is equivalent to stating that the coldest conditions occur when perihelion occurs on November 19. We refer to the aphelion date in this case because we believe the spring insolation is the controlling influence.) The substantial fraction of annual mean SAT variance associated with precession is significant, given that precession has no effect on annual mean insolation. This implies that changes in insolation due to precession during some portion of the year must have a disproportionate effect on annual mean SAT.

Evidence for this disproportionate response can be seen in the seasonality of the response of zonal mean SAT to orbital forcing (Fig. 3). The response to precessional forcing is depicted by choosing an aphelion date of May 20th, which is the phasing that minimizes annual mean Arctic SAT (60°N–90°N). The corresponding sensitivity of insolation to obliquity and precessional forcing is shown by contours within the same figure.

One of the most striking features of this analysis is the counterintuitive response of the Arctic SAT to precessional forcing, which is dominated by cooler temperatures through much of the year, even during those seasons when insolation is increased. This contrasts with the low-latitude response, in which SAT exhibits a 1–2 months delay relative to the seasonal cycle of insolation anomalies. This contrast is depicted in a polar coordinate diagram that shows both the amplitude and phase of SAT sensitivity to precessional forcing for each month of the year (Fig. 4a). The longitude of the perihelion (defined to be zero when perihelion occurs on the autumnal equinox) that maximizes SAT for a particular month is given by the angle with respect to the polar axis. The distance from the center of the circle depicts the amplitude of the sensitivity. For SAT averaged between 70°N to 90°N, virtually all of the monthly amplitude-phase positions lie in the lower left portion of the plot (Fig. 4a), indicating that cold anomalies occur throughout much of the year when aphelion is in spring (i.e., perihelion in autumn). This contrasts with the behavior of SAT averaged between 20°N to 40°N (Fig. 4b), which responds more linearly to precessional

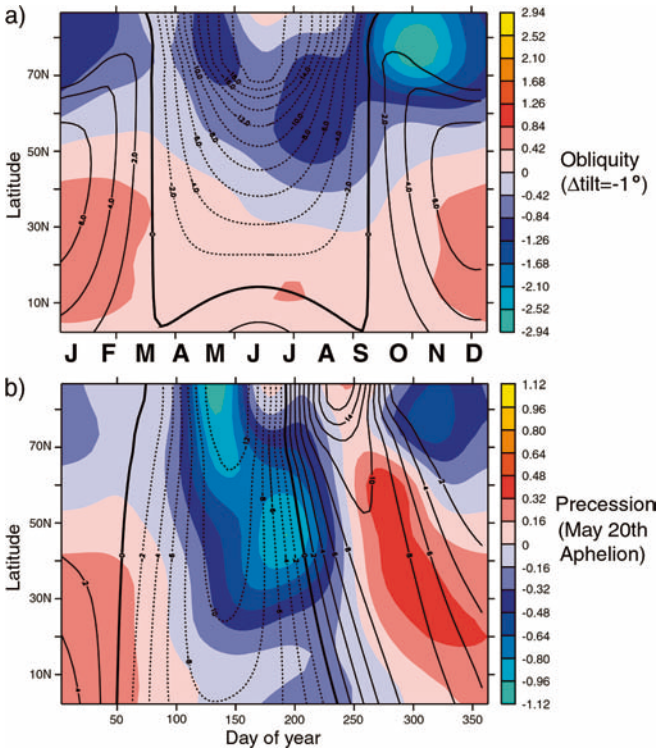

Fig. 3 Seasonal sensitivity of zonally averaged surface air temperatures (*colors*; *blue*, cooling, *red*, warming) and insolation (contours, interval is 2 W/m^2) to **a** obliquity forcing and **b** precessional forcing. Sensitivity to obliquity is given by the temperature anomaly (with respect to the long-term mean) that occurs in response to a 1° reduction in obliquity (i.e. $-\mathbf{A}_o$ of Eq. 1). Sensitivity to precession is given by the temperature anomaly that results from setting the longitude of the perihelion to a given value and arbitrarily assuming an eccentricity of 0.01. In this instance, the longitude of the perihelion is set to 59°, which places perihelion on November 19th and aphelion on May 20th

forcing. At these latitudes, maximum SAT for a particular month is associated with the occurrence of perihelion about 1–2 months earlier, which is consistent with the thermal inertia provided by the mixed-layer ocean.

The seasonal and annual mean response of Arctic SAT to orbital forcing as demonstrated in Figs. 2–4 can ultimately be related to three properties of the Arctic that are affected by the presence of sea ice: (1) the long equilibration time of the Arctic, (2) the seasonality of SAT sensitivity to forcing, and (3) the rectification of insolation variations by sea-ice albedo feedbacks.

The long equilibration time of the northern high latitudes is important to damping the effect of seasonal variations in orbital forcing on SAT. Sea ice can be regarded as a reservoir of negative thermal energy, which is equivalent to an enhancement of thermal inertia and thus slows the response of the high-latitude climate system. Sea ice also damps the exchange of energy between the atmosphere and the mixed-layer ocean. In combination, these characteristics of sea ice can lengthen the equilibration time of the northern high latitudes by several years. This length of time is sufficient to allow forcings or processes that affect annual mean SAT to also dominate seasonal variations in SAT.

As for the second property, the seasonality of SAT sensitivity over the Arctic basin is largely controlled by feedbacks involving sea ice. The sensitivity is weakest during summer when surface melting of sea ice constrains SAT to be close to 0 °C irrespective of orbital configuration. The largest sensitivity occurs in late autumn and early winter, shortly after sea-ice extent and thickness reach their seasonal minima. During this season, SAT is especially sensitive to sea-ice thickness and extent as the ice insulates the rapidly cooling lower atmosphere from the warmer (i.e., near-freezing) ocean water below (Ledley and Pfirman 1997; Manabe and Stouffer 1980). Thus, sea ice feedbacks cause the

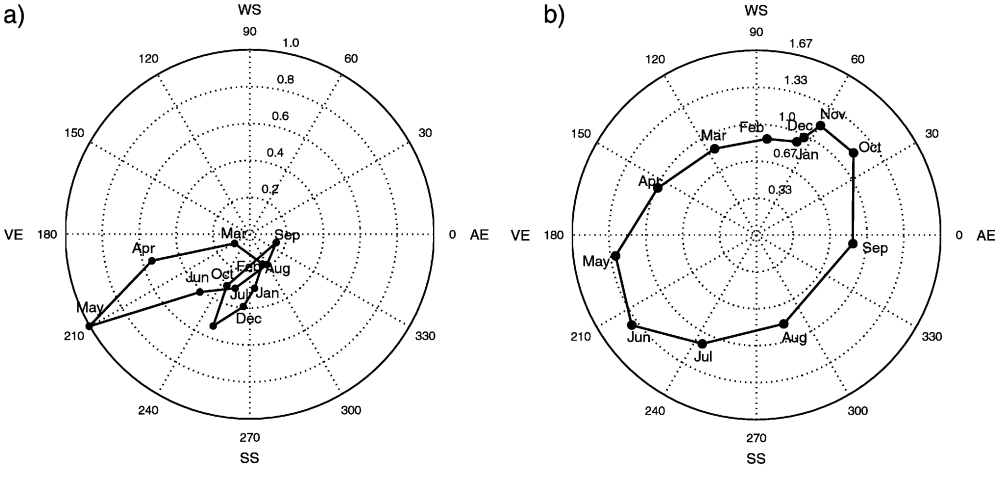

Fig. 4 Polar coordinate diagrams of the monthly mean sensitivity of spatially averaged surface air temperature **a** 70°N to 90°N and **b** 20°N to 40°N. The *angle* indicates the longitude of the perihelion for which the temperature in a given month is maximized (i.e., ϕ_p in Eq. 1), and the radial distance indicates the magnitude of the temperature anomaly for that perihelion longitude if eccentricity is assumed to equal 0.01 (i.e., $0.01\mathbf{A}_p$ in Eq. 1). Units are K. For example, the spatial mean temperature for 70°N to 90°N during May is a maximum when the longitude of the perihelion is 210° and the temperature anomaly under such conditions is 1 K if the eccentricity is 0.01

seasonal SAT responses to obliquity and precessional forcing to be quite similar despite the different effects of these forcings on the seasonal and annual mean insolation. This similarity is also evident in the geographical distribution of SAT response for many months of the year (not shown), which show similar spatial structures resulting from obliquity and precessional forcing, including a wave 2 pattern reflecting cooler temperatures over the high latitude ocean and warmer temperatures over the continents.

Finally, the effect of sea ice albedo feedbacks on the rectification of insolation anomalies is important to enhancing the amplitude of the response of SAT to orbital forcing. This is most evident for the precessional component of orbital forcing which has no effect on annual mean insolation. Radiative feedbacks involving sea ice are essential in this rectification process, as they amplify the effects of insolation changes during the late spring melt season, when the surface albedo is quite sensitive to changes in radiative input (Ledley and Pfirman 1997). The phase lag between the seasonal cycle of insolation and surface climate is critical to the rectification process because it allows extensive ice to coexist with near-freezing temperatures and high insolation in spring. A similar sensitivity does not exist in autumn because insolation is much weaker at the times when the same combination of temperatures and cryospheric conditions is present. An evaluation of the relative size of radiative feedbacks involving sea ice, snow cover, and clouds at all latitudes is considered next.

5 Radiative feedbacks

To better understand the processes involved in orbitally forced climate change, anomalies in the net shortwave radiation received at the top of the atmosphere at a given phase of the seasonal cycle can be partitioned into a radiative forcing term and a radiative feedback term. For a given phase of the seasonal cycle, the top-of-atmosphere (TOA) shortwave radiation budget can be expressed as

$$Snet = S(1-\alpha) \tag{2}$$

where *Snet* is the net TOA shortwave radiation, S is the TOA incident radiation, and α is the TOA albedo. Each of these quantities can be represented as the sum of a long-term mean and time-varying anomaly, such that the anomaly in *Snet* can be expressed as

$$Snet' = S'(1-\bar{\alpha}) - (\bar{S}+S')\alpha' \tag{3}$$

where the overbar indicates a long-term mean and the primed quantities represent the anomalies with respect to the long-term mean. The first term on the right hand side of Equ. (3) is the radiative forcing, which is the effect of the orbitally induced insolation anomalies on the radiation budget of the unperturbed climate. The second term represents the radiative feedbacks in which changes in climate (specifically, those resulting in a change in TOA albedo) further modify the TOA radiation budget.

To obtain annually averaged values for the forcing and feedback terms, Eq. (3) is integrated over the seasonal cycle. The obliquity and precessional components of zonal and annual mean insolation, forcing, and feedbacks are obtained using the decomposition method described in Sect. 4 (Fig. 5). As required by Eq. (3), the latitudinal distribution of obliquity forcing (Fig. 5a) is similar to that of obliquity-induced insolation anomalies, with a 2 to 3 W/m^2 decrease in radiation received at high latitudes and a 1 to 2 W/m^2 increase in radiation received at low latitudes. Forcing is reduced relative to insolation, with the largest reduction occurring at high latitudes where the annual mean $\bar{\alpha}$is largest. For most latitudes, shortwave radiative feedbacks resulting from obliquity changes are of the same sign as the forcing, amplifying the changes in the pole-to-equator gradient

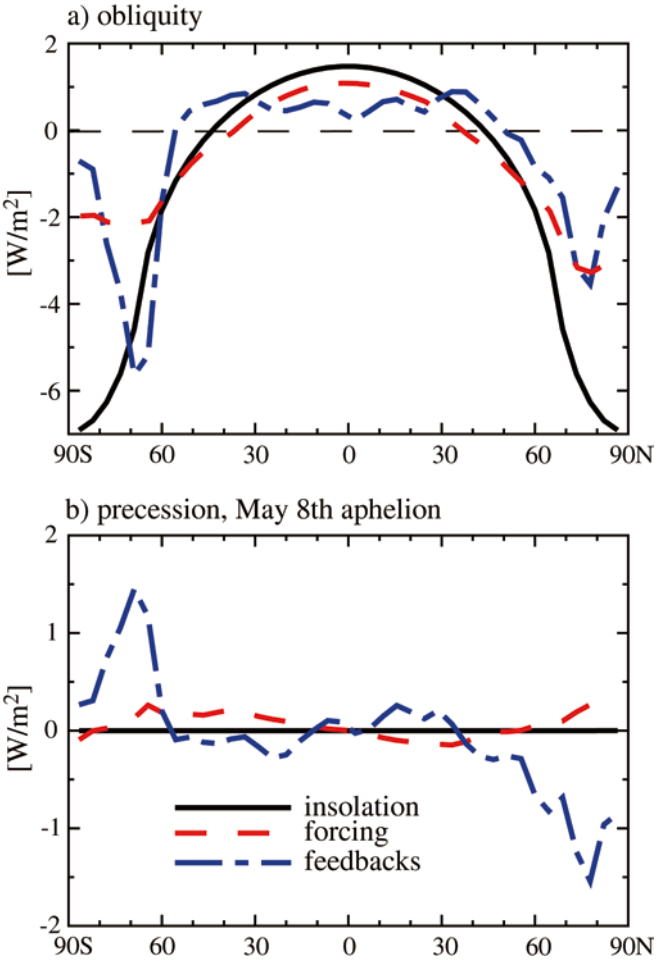

Fig. 5 Latitudinal profile of the sensitivity of annual mean insolation (*solid black*), forcing (*dashed red*), and feedbacks (*dot dashed blue*) to **a** obliquity forcing **b** and precessional forcing with the longitude of perihelion λ set to November 7th (May 8th aphelion) the date that maximizes annual mean feedbacks in the Arctic. Forcing and feedbacks are defined in Eq. 2. Sensitivity is defined within text of Sect. 4

of radiation received. The feedbacks are similar in magnitude to the forcing, except in high austral latitudes, where the feedbacks are up to three times as large.

The precessional sensitivity (Fig. 5b) is shown with the longitude of the perihelion set to November 7th (i.e., May 8th aphelion), a choice that maximizes the size of the radiative feedbacks in the Arctic. (Note that this date is close to the May 20th aphelion date that minimizes annual mean SAT for this region.) Because the annual mean insolation is insensitive to precession, the existence of a nonzero annual mean precessional forcing indicates that the seasonal variations in $\bar{\alpha}$act to rectify the seasonal insolation anomalies. Unlike the sensitivity to obliquity, the precessional forcing is rather small compared to the feedbacks, particularly at higher latitudes. Because the characteristics of spring sea ice make it very sensitive to insolation changes (as discussed in the previous section), there is a large decrease in radiation received when aphelion is on May 8th, as the shortwave radiative feedbacks overwhelm the weak positive annual mean forcing. In low latitudes, precessional feedbacks are smaller and have opposite sign from those at high latitudes. The feedbacks are anti-symmetric across the equator, consistent with the seasonal response of insolation to precession.

The feedbacks attributed to precession and obliquity are quite large. During the period from 100–130 ka, when eccentricity was near is maximum value ($\backsim 0.04$), the annual mean radiative feedbacks occurring in high latitudes during extremes in the precession cycle are approximately 6 W/m^2, and are comparable in size to the 4–6 W/m^2 feedbacks associated with a 1° reduction in obliquity. For comparison, a doubling of CO_2 results in maximum shortwave radiative feedbacks of 10–14 W/m^2 in high latitudes in the very similar model used by Broccoli (2000). Thus the effects of orbital variations on the shortwave radiative climate of the Arctic are relatively strong.

Only changes in clouds, sea ice, and snow can affect shortwave radiative feedbacks within the current model design. Some indication of the relative size of the snow and sea ice feedbacks at high latitudes can be inferred from the sensitivity of surface albedo to obliquity and precessional forcing (Fig. 6). As in the forcing and feedback analysis, aphelion on May 8th is chosen as the reference orbital configuration. Changes in land albedo are indicative of snow feedbacks, while changes in ocean albedo are indicative of sea-ice feedbacks. The largest change in surface albedo occurs at high latitudes, with large increases in surface albedo where radiative feedbacks are also the most negative. Sea ice feedbacks tend to dominate snow feedbacks in the polar latitudes with increasing importance to snow feedbacks in the midlatitude Northern Hemisphere, where snow feedbacks are out of phase with those at higher latitudes. The out-of-phase response of midlatitude snow is a consequence of the relatively rapid response of the continents to the increases in winter insolation that occur for both low obliquity and spring aphelion.

There is little or no sensitivity of surface albedo between approximately 50°S and 25°N. Thus any

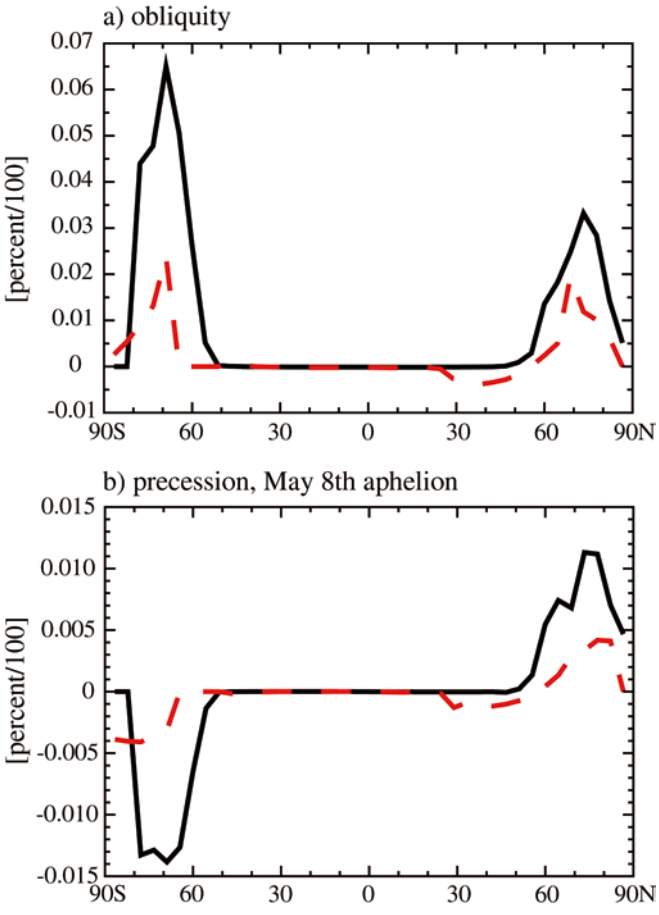

Fig. 6 Latitudinal profile of the sensitivity of annual mean surface albedo averaged over sea points (*solid black*) and land points (*dashed red*) to **a** obliquity forcing and **b** precessional forcing with longitude of the perihelion set to November 7th (May 8th aphelion)

feedbacks that occur within this latitude band must be occurring through changes in cloud cover. There are significant changes in cloud cover at all levels in response to obliquity and precessional forcing (not shown). For the obliquity component there are reductions in low clouds at all latitudes except near the equator, decreases in middle clouds in the extratropics, a slight increase in middle clouds in the tropics, and increases in high clouds at all latitudes. The cloud changes in the tropics and subtropics appear to be related to an increase in the strength of the Hadley cell, with small increases in mid-level clouds corresponding to the location of the annual mean intertropical convergence zone, and decreases in low and middle clouds corresponding to the two downwelling branches of the Hadley cell in the subtropics. Cloud forcing diagnostics suggest that the net radiative effect of these cloud changes is primarily to shortwave rather than longwave radiation.

The response of clouds to precessional forcing (again using aphelion on May 8th as the reference orbital configuration) is generally antisymmetric between the hemispheres. Decreases in low clouds in the northern tropics and subtropics are consistent with the weakening of the summer monsoon. An increase in clouds in the

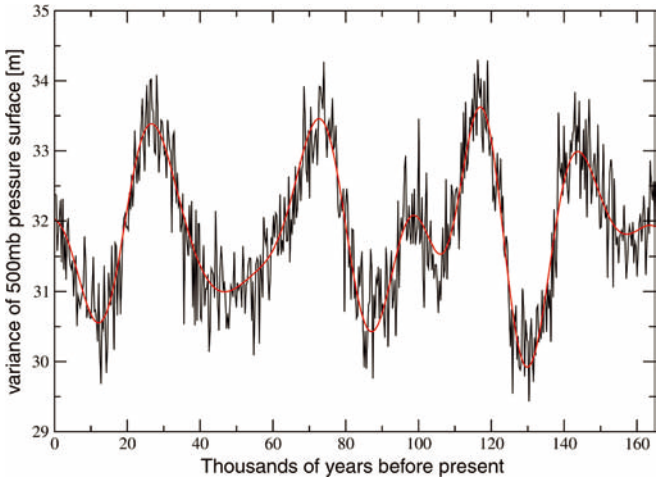

Fig. 7 Time series of annual mean storm activity (2.5 to 6 day bandpass filtered variance of 500 mb pressure surface) averaged between 45°N and 65°N. Each *point* represents a 10-year mean from the model integration. The *red curve* represents the best linear fit between obliquity and precessional variations and the time series

midlatitude Northern Hemisphere, extending downward almost to the surface, accompanies an increase in wintertime storm activity, which will be discussed at greater length in the following section. A reduction of low and middle clouds occurs in the Arctic, presumably in response to the colder, and hence drier, conditions there. As in the case of obliquity forcing, cloud forcing diagnostics suggest that the radiative effects of these changes in cloud cover are dominated by their effect on shortwave radiation.

6 The latitudinal temperature gradient and its effect on storm activity

Changes in surface climate are intimately related to changes in large-scale circulation, including the number and intensity of storms that we term 'storm activity'. One measure of storm activity is the 2.5 to 6 day bandpass-filtered variance of the height of the 500 mb pressure surface (Blackmon 1976). The time series of annual mean storm activity averaged between 45°N and 65°N exhibits the influences of obliquity and precession (Fig. 7). Storm activity is maximized when obliquity is low and perihelion is on November 13th (May 14th aphelion) (Table 1). The contrast between the high-latitude and low-latitude SAT responses to orbital forcing has a significant impact on the strength of the zonal winds and storm activity. As was noted earlier, orbital configurations in which obliquity is low or aphelion is in late spring aphelion result in relatively large high-latitude cooling in late fall and early winter (Fig. 3). Insolation anomalies associated with this orbital configuration also warm the low latitudes during the same season. As a consequence, low obliquity and late spring aphelion lead to the largest enhancement of the

Table 1 Sensitivity of select quantities to changes in obliquity and precession

	June insolation 65°N (W/m^2)	Annual mean surface air temperature 60–90°N (°K)	Annual mean radiative feedbacks 60–90°N (W/m^2)	Annual mean storm activity 45–65°N (m)	Annual mean ablation NE Canada (positive degree-days)	Annual mean snowfall NE Canada (m/day)
Obliquity sensitivity $-\mathbf{A}_o$ (percent variance)	15.8 (21.3)	0.93 (51.1)	2.0 (30.1)	–1.1 (54.8)	107.5 (33.1)	-0.33×10^{-4} (29.3)
Precession Sensitivity 0.01 times $\mathbf{A}_p$ (percent variance)	10.0 (79.9)	0.28 (42.5)	0.99 (67.1)	0.24 (24.6)	47.8 (61.0)	0.13×10^{-4} (40.5)
Phase of longitude of Perihelion ϕ_p	262°	239°	227°	52°	241°	33°
Phase of obliquity that is most glaciation friendly	NA	Low	Low	Low	Low	Low
Date of perihelion and aphelion that is most glaciation friendly	NA	Perihelion on November 19th Aphelion on May 20th	Perihelion on November 6th Aphelion on May 8th	Perihelion on November 11th Aphelion on May 14th	Perihelion on November 20th Aphelion on May 22nd	Perihelion on October 23rd Aphelion on April 24th

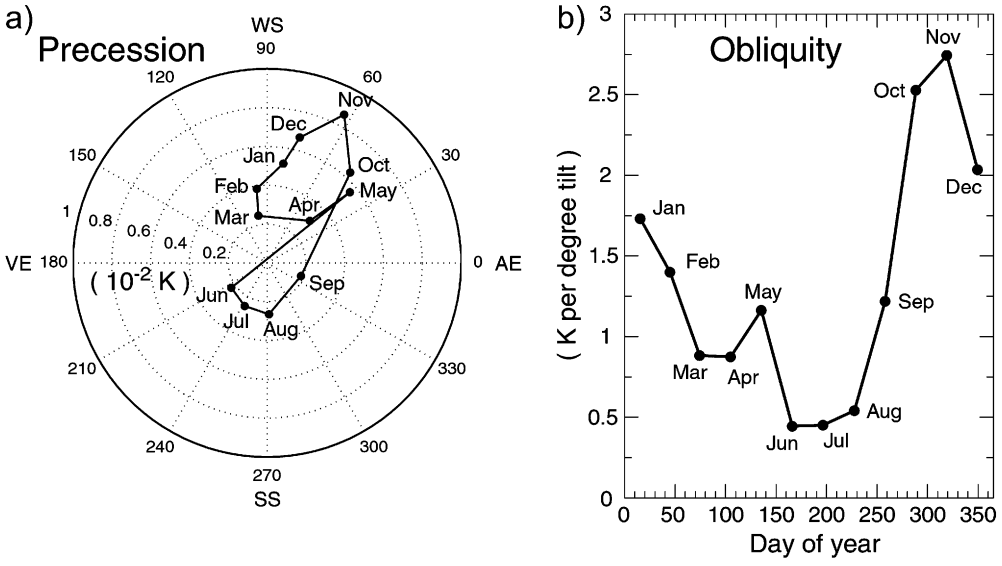

Fig. 8 Monthly mean sensitivity of latitudinal temperature gradient (20°N–40°N minus 70°N–90°N) for **a** precessional forcing where phasing on dial corresponds to longitude of perihelion and amplitude by the distance from center of circle and **b** obliquity forcing where obliquity has been reduced by 1°. Note that aphelion is a half-year offset from perihelion. Therefore, a late autumn perihelion has the same orbital configuration as a late spring aphelion

pole-to-equator SAT gradient between October and January (Fig. 8).

Maps of the sensitivity of the October through January mean height of the 500 mb pressure surface to obliquity and precessional forcing (with the perihelion date set to November 11th, the date that maximizes annual mean storm activity) indicate that the enhanced meridional temperature gradient at the surface is accompanied by an increase in the meridional pressure gradient and an increase in the mean westerly flow in the midlatitudes (Fig. 9). These changes are consistent with the thermal-wind relationship that relates meridional SAT gradients to vertical wind shear. For this reason, an enhanced SAT gradient generally leads to enhanced storm activity which derives from the accumulation of potential energy to the south of the zonal wind anomalies (as can be seen through the increase in geopotential height to the south of the enhanced westerlies) as well as tendency for increases in the vertical wind shear to support the faster growth of unstable modes (storms) within the atmosphere. Indeed, these changes in SAT, upper level flow, and geopotential height are associated with a widespread high latitude increase in storm activity (Fig. 10). Note that there are discernable decreases in storm activity in the subtropics, particularly in the precessional response over Southeast Asia, that are likely related to decreases in westerly winds in the same latitude band.

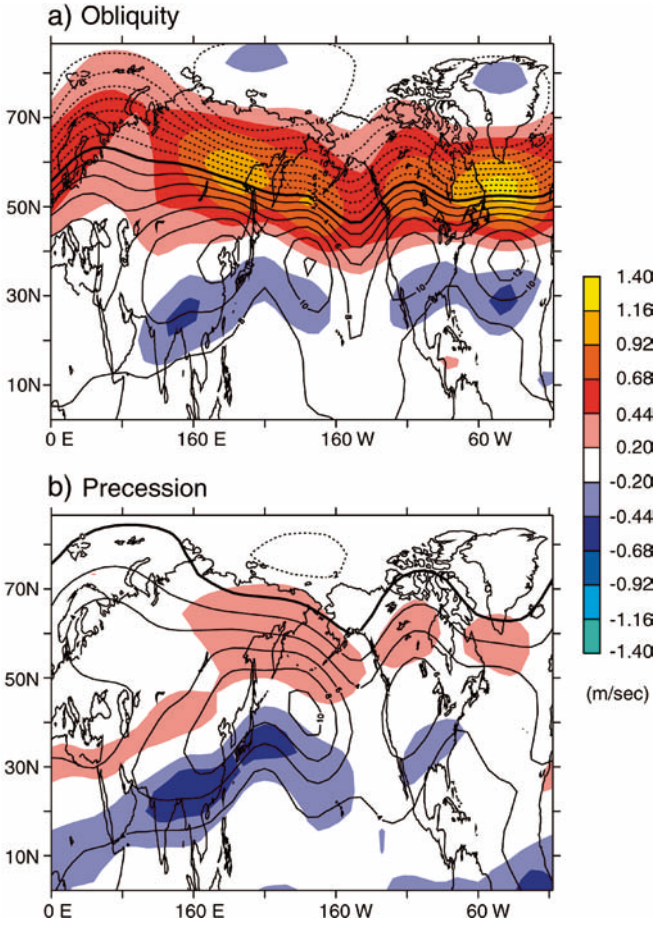

Fig. 9 October through January mean sensitivity of zonal winds (color) and 500 mb geopotential (contours) for **a** obliquity forcing and **b** precessional forcing with the longitude of the perihelion set to November 11th (May 14th aphelion). Units for zonal winds are m/s. Units for geopotential are in m. The geopotential contour interval is 2 m

7 Poleward heat transports

One potentially useful diagnostic of the atmosphere in its response to orbital forcing is an evaluation of the effects of this forcing on the partitioning of poleward heat transports by the mean meridional circulation (*MMC*), transient eddies (*TE*), and stationary eddies (*SE*). All poleward heat transports must take place through some combination of these circulations. The

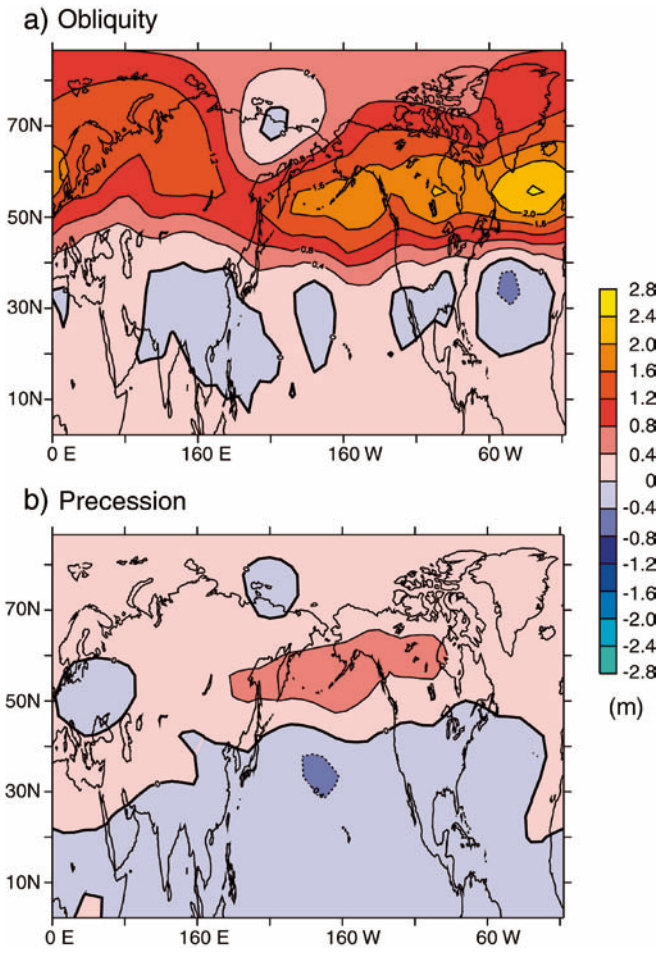

Fig. 10 October through January mean sensitivity of storm activity (2.5 to 6 day filtered variance of 500 mb pressure surface) **a** obliquity forcing **b** precessional forcing with the longitude of perihelion set to April 24th. Units for storm activity are in m

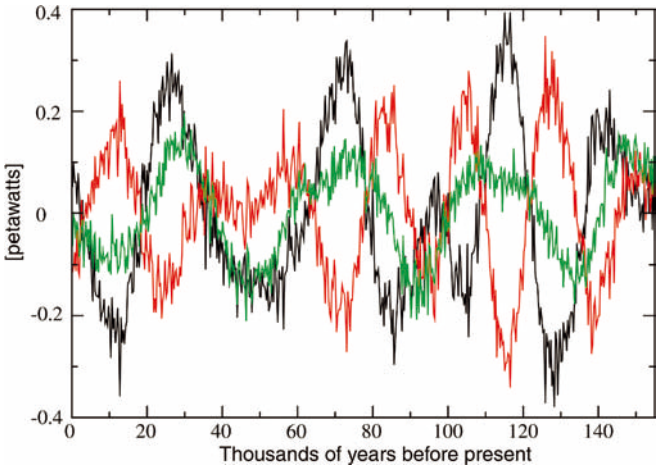

Fig. 11 Annual mean poleward energy transport anomalies at 45°N by transient eddies (*black*), stationary eddies (*red*), and the sum of transient and stationary eddies (*green*). Units are in petawatts (10^{15} W). Note that time series ends at 155 ka owing to an unresolved irregularity in calculated fluxes for dates beyond 155 ka

total heat transport budget is constrained by the difference in the radiative surplus at low latitudes and the radiative deficit at high latitudes. Because orbital forcing, and obliquity forcing in particular, affects the latitudinal distribution of radiation incident at the TOA one may anticipate that orbital forcing affects the total budget as well.

The description of how *MMC*, *TE*, and *SE* components of poleward heat transports are determined is found in the Appendix. The annual mean poleward energy transport anomalies at 45°N by *TE*, *SE*, and their sum are given in Fig. 11. The sum of energy transports by *TE* and *SE* accounts for the majority of the anomalies with a small fraction attributed to changes in the *MMC*. The consistent $\backsim$40 ky periodicity of *TE* + *SE* time series shows the dominance of obliquity on mean changes in the energy transport budget. As expected, the maxima in *TE* + *SE* transports occur around 29, 70, 112, and 150 ka when obliquity is low. What is also apparent in Fig. 11 is a large compensation between the *SE* and *TE* partitioning of the poleward energy transports with amplitude twice as large (near 115 ka) as the changes in the mean budget due to obliquity variations. The maxima in the *TE* component occurs approximately around the same time intervals that we noted earlier that have the lowest annual mean air temperatures for the Arctic (i.e., 26, 73, 117 ka). These maxima are accompanied by a significant reduction in the SE component on both obliquity and precessional time scales. The precessional component has nearly equal and opposite amplitude variations of *TE* and *SE* with maxima in TE occurring when aphelion is on June 11th and a sensitivity of 4.5×10^{13} W (the sensitivity as defined in Sect. 4) and minima in *SE* occurring when aphelion is on June 21st and a sensitivity of 5.2×10^{13} W. When obliquity is low, *TE* component increases by 1.8×10^{14} W and *SE* component is reduced by 7.0×10^{13} W. Therefore, the nearly equal and opposite response between *SE* and *TE* components from precessional forcing allows obliquity to dominate annual mean variations in total energy transport at 45°N.

The range in the *TE* anomalies is 16% of its long-term mean of 4.1×10^{15} W, which is consistent with the percent change in seasonal insolation due to orbital forcing. The range in the *SE* anomalies, however, is 60% of its long-term mean of 8.7×10^{14} W. The nature of the compensation between *SE* and *TE* components and the extraordinarily large response of *SE* to orbital forcing warrants some further exploration. Although a complete understanding of these features is beyond the scope of the present analysis, we can get some notion of how these changes occur by: (1) considering the seasonal breakdown of the response of each of these components to obliquity and precessional forcing; (2) checking to see if the zonal mean and regional response of storm activity and 500 mb stationary waves are consistent with the changes in the *SE* and *TE* heat transport components, and (3) evaluating the relative importance of the

poleward transport of potential energy, latent heat, and sensible heat for each of the *SE* and *TE* components.

The compensation between the *SE* and *TE* occurs during two segments of the seasonal cycle (not shown); a summer segment centered around the month of July and a winter segment centered (roughly) around the month of December for both obliquity and precessional components. The winter segment is likely responding, at least in part, to the enhanced meridional temperature gradient and associated enhancement of mid-latitude storm activity (see preceding section) thereby allowing for more of the total poleward heat transport budget to take place through *TE*. However, the increase in *TE* component during the summer segment takes place when the zonal-mean meridional temperature gradient is reduced or near its annual minimum (Fig. 8).

Maps of the reduced *SE* component of poleward heat transports during July indicate that the majority of the heat transport anomalies are local to Southeast Asia. This observation is corroborated by a 20% reduction in stationary wave amplitude at the same location. Maps of storm activity show about a 10% increase over the mid-latitude Pacific Ocean that extends across North America and Atlantic Ocean. The origin of this increase in storm activity is local to Southeast Asia and, presumably, is related to the same processes affecting the change in stationary waves or even the stationary waves themselves. This same mechanism could also be a part of the wintertime response as well as is corroborated by a reduction in the stationary wave amplitude over Southeast Asia and western Pacific, although this inference is not as apparent since the reduction in stationary wave amplitude and *SE* component of poleward heat transports occur throughout the mid-latitudes.

One may decompose further the heat transport anomalies into contributions from potential energy, sensible heat, and latent heat. At 45°N, most of the poleward energy transport takes place through the sensible and latent heat components. In July, the majority (over 90%) of the *SE* anomalies come from latent heat transports. In December, the situation is reversed with the majority of the *SE* anomalies coming from sensible heat and potential energy transports. No such dominance exists within the *TE* components, as the changes in sensible heat and potential energy transport are equally large as those due to latent heat transport for both July and December. It is interesting to note that the range in latent heat transports for *SE* is over 160% of its mean in July and over 60% of its mean in December. This fact, in conjunction with the identified importance of processes occurring near Southeast Asia mentioned, strongly suggests that the *SE* and *TE* components of poleward energy transports are being modulated by the Southeast Asian Monsoon. When aphelion occurs during summer and obliquity is low, the orbital configuration that minimizes the *SE* component and maximizes the *TE* component, the amplitude of the Asian summer 'wet' monsoon is greatly reduced which, we infer, reduces the monsoon's role in the poleward transport of moisture and its forcing of stationary waves within the atmosphere. The situation would be reversed during winter for this orbital configuration as heating of the continental interior reduces the temperature and pressure contrast between the Asian continent and the warmer Indian Ocean which would minimize the amplitude of the winter 'dry' monsoon and its ability to force stationary waves within the atmosphere. The large percent change in the *SE* component is consistent with earlier studies that show the ability of the Asian monsoon to focus the effects of orbital forcing into a concentrated area (Prell and Kutzbach 1987). Here we see how this focusing could potentially have wider impacts on the general circulation and storm activity in particular.

We do not know for certain if changes in the *SE* component of poleward heat transports are forcing the compensating changes in the *TE* component. We showed in the preceding section how increases in the meridional temperature gradient during winter correspond to a widespread increase in storm activity. This increase in storm activity would presumably also increase the amount of poleward heat transports and, by necessity, reduce the relative importance of heat transport by stationary waves. Also, there is some evidence that increases in the meridional temperature gradient can cause reductions in stationary wave amplitude (Cook and Held 1988). These relationships, however, cannot explain the increases in storm activity and reduced stationary wave amplitude that we found during summer when the zonal-mean meridional temperature gradient is at a minimum. It could be that the relative importance of the Asian monsoon or the changes in the meridional temperature gradient on the partitioning between *SE* and *TE* components is seasonally dependent.

8 Implications for glaciation

In this section, we present an analysis of processes affecting ablation and snowfall over northeastern Canada (NE Canada: land points 100-60°W, 60–75°N), a region associated with the initiation of the Laurentide ice sheet. To a large extent these findings also hold for the location of the Fennoscandian ice sheet that covered northwestern Eurasia (NW Eurasia: land points 0–90°E, 60–75°N). However, there are some potentially important differences between these two regions that will be discussed in the following section. Here we present analyses of ablation and snowfall in terms of tendencies or qualitative assessments of how various processes are contributing or inhibiting either of these quantities. The interconnected nature of thermodynamics and dynamics within the atmosphere makes it difficult to separate out processes in each of these categories in a budgetary sense. Where possible, we will point out the prominence of one process over another.

We cannot evaluate variations in ablation directly since our model does not contain glacier dynamics.

Thus, the regions of permanent land ice are prescribed in their present locations throughout the climate model integration. Instead, we estimate orbital effects on ablation by using the annual sum of positive daily temperatures, or positive degree-days (PDD), which are observed to be proportional to ice melt rates (Braithwaite 1995).

For NE Canada, the climate model simulates prominent minima in PDD at 26, 73, and 117 ka and secondary minima at 97 and 142 ka (Fig. 12). The prominent minima in PDD occur during periods when obliquity is low and aphelion is in late spring (and perihelion occurs during the late fall season), both of which contribute to reduced summer insolation. Approximately concurrent with these minima in PDD are prominent maxima in snowfall at 27, 74, and 118.5 ka with secondary minima at 99 and 142.7 ka (Fig. 12). Therefore, ablation and snowfall together contribute to "glaciation-friendly" conditions during similar time intervals. As summarized in Table 1, the optimal orbital configuration for glaciation occurs when obliquity is low and aphelion in late spring. The percent variance accounted for by obliquity is comparable to precession for both PDD and snowfall with precession being more important to PDD (61% of the variance) than for snowfall (40.5% of the variance).

Also shown in Fig. 12 are two reconstructions of eustatic sea level which corresponds to the growth and decay of continental ice sheets. Sea level reconstructions are only approximate since there can be multiple factors contributing to the reconstructions. The difference between the two curves gives some sense of the uncertainty in both the timing and amplitude of past sea level variations. The most prominent feature of the sea level curves is the large $\backsim$100 ky variation in sea level. There is no corresponding $\backsim$100 ky feature within the model derived fields for ablation or snowfall forced by changes in orbital geometry. The correspondence may improve if we had included CO_2 forcing in addition to changes in orbital geometry, however it is evident that the 100 ky glaciation cycle is not related in a simple manner to the direct effects of eccentricity on insolation (Imbrie et al. 1993). On obliquity and precessional time scales however, there is a clear correspondence between the decreases in ablation increases in snowfall and periods of falling sea level near 27, 75, 115 ka and a period of modest sea level fall around 95 ka.

In order to interpret how orbital forcing affects time intervals that are most conducive for glaciation we draw upon the understanding we have gained within previous sections on the large scale (zonal mean) processes affecting SAT and storm activity and evaluate how orbital forcing is affect the climate over the specific region of NE Canada. The following synthesis will rely on Fig. 13 which shows the seasonal precessional and obliquity sensitivities for insolation, snow fall, SAT, precipitation, storm activity, and snow fraction over NE Canada for the most optimal orbital configuration for glaciation (April 24th aphelion, and low obliquity).

The above-freezing seasonal changes in SAT, which control the amount of ablation that occurs during a year as indicated by the PDD relationship, does not exactly follow the local changes in insolation. Rather, the changes in SAT appear to be consistent with the analysis of zonal mean SAT that is strongly influenced by radiative feedbacks operating in late spring and the long equilibration time scale of the high northern latitudes. Therefore, the most important reason summer insolation may be important to the waxing and waning of glacial cycles may not because of the direct effect of

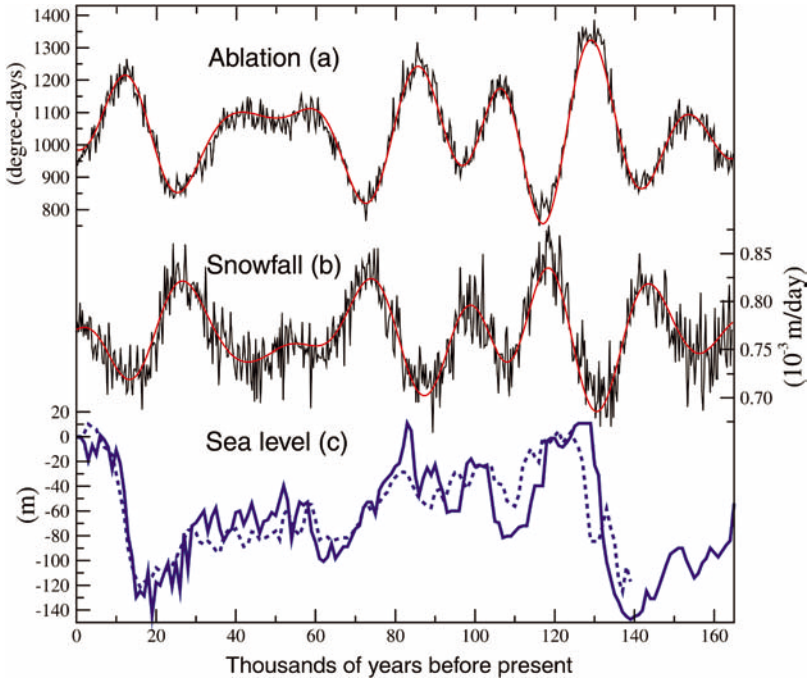

Fig. 12 Time series comparison of model predictions of **a** ablation and **b** snowfall over NE Canada with **c** two marine records of sea level variations for the last 165,000 years (*solid line*, Shackleton 2000; *dashed line*, Shackleton 1987). Each point represents a 10-year mean from the model integration. The *red curve* represents the best linear fit between obliquity and precessional variations and the time series

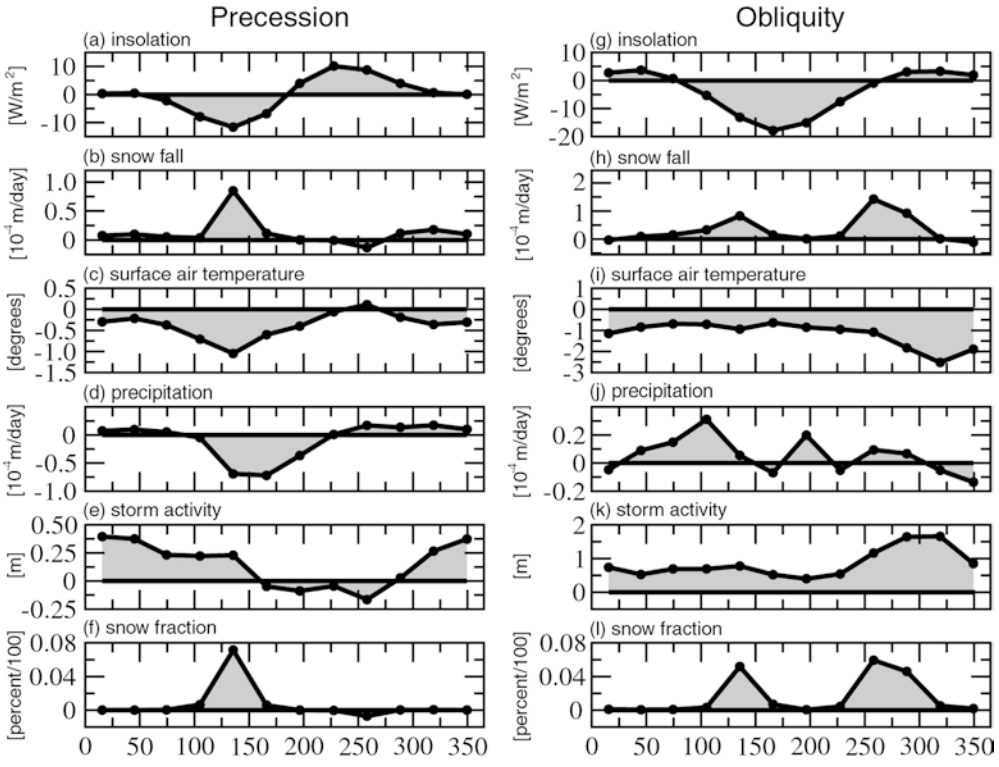

Fig. 13 Monthly mean sensitivity of insolation (**a** and **g**), snowfall (**b** and **h**), surface air temperature (**c** and **i**), precipitation (**d** and **j**), storm activity (**e** and **k**), and snow fraction (**f** and **l**). *Left column* shows sensitivity to precessional forcing with the longitude of perihelion set to April 24th. *Right column* shows sensitivity to obliquity forcing

insolation on ablation, but rather the indirect effect of insolation on changes in sea ice and snow cover and the thermal properties of the high northern latitude ocean.

Snowfall variations over NE Canada result from both dynamical and thermal effects. The dynamical effects of a late spring aphelion are most apparent between November and April when increases in storm activity counteract the tendency for high-latitude precipitation to be inversely correlated with temperature. A low obliquity enhances storm activity throughout the year, particularly in late autumn, and contributes to the dynamical effects of orbital forcing on annual mean snowfall variations. The largest thermal effects of a late spring aphelion are most apparent in May when reductions in SAT lead to increases in snow fraction (the fraction of precipitation falling as snow). Obliquity effects snowfall similarly, but includes large increases in snow fraction during fall as well.

9 Processes affecting regional variations in snowfall

Emphasis up to this point has been on describing the large-scale or zonal mean response to orbital forcing and examining how this response affects NE Canada. These conclusions are largely valid for NW Europe. There are, however, zonal asymmetries that are important in determining slight differences in the phase of the longitude of the perihelion that maximizes snowfall for these two regions. The main source of zonal asymmetries is stationary waves within the atmosphere. Model predictions of changes in the stationary wave field due to orbital forcing are probably model dependent and specific conclusions regarding their role in glacial-interglacial cycles should not be given much weight. Even so, the model results can be used to illustrate the unique role stationary waves can play in creating apparent leads or lags within the precessional component of glacial cycle time series. These apparent phasing differences can lead or lag the primary (zonal mean) response by thousands of years despite the fact that they occur within a climate system model that does not contain the deep ocean's long-term memory. Such regional differences usually have some dynamic significance and, if observed within the geologic record, could provide important clues of the climate system's dynamic response to orbital forcing.

Consider the similarities and differences between annual mean snowfall variations in NE Canada with those in NW Eurasia (Fig. 14). Both time series have maximum snowfall when obliquity is low and aphelion is in spring and similar proportions of precession and obliquity (39.7% and 25.3%, respectively. See Table 1 for values for NE Canada). The main difference between the two time series can be seen in the apparent 2.5 kyr lead of maximum snowfall in NW Eurasia with respect to the maximum in NE Canada. Because there is no glacier dynamics within the model, this phase difference cannot be attributed to the growth of ice sheets in NW Eurasia affecting snowfall in NE Canada. Rather, the difference in phasing is a result of the fact that snowfall is maximized when aphelion is on March 9th in NW Eurasia and it takes 2.5 kyr before aphelion is on April 24th and snowfall is maximized over NE Canada. The phasing of

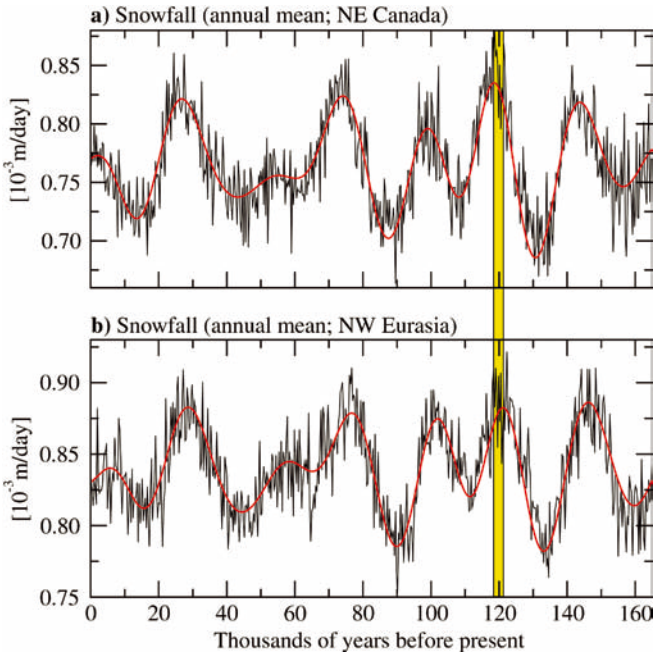

Fig. 14 Annual mean snowfall over NE Canada **a** and NW Eurasia **b**. The *left edge* of *yellow column* indicates time of maximum snowfall around 118 ka over NE Canada. *Right edge* of *yellow column* indicates time of maximum snowfall around 121 ka

annual mean snowfall with respect to the longitude of the perihelion for each of these regions is dominated by the response during May which is very similar between NE Canada and NW Eurasia. The responses during other seasons are also very similar except for the month of October when there is a significant reduction in snowfall over NW Eurasia and modest increase in snowfall over NE Canada. This difference in the response during October accounts for majority of this 2.5 kyr phasing offset.

We have considered Northern Hemisphere maps of October mean sensitivity to an April 24th aphelion precessional forcing for snowfall, SAT, precipitation, stationary wave field, zonal winds, storm activity, and poleward latent heat transport (not shown) to examine what processes are favoring snowfall over NE Canada and disfavoring snowfall over NW Europe. The anti-correlation between changes in precipitation and SAT for these regions suggests dynamics is more important than the role of SAT on the saturation vapor pressure (when precipitation would tend to be correlated with SAT) for explaining the changes in snowfall. The primary source for these regional differences is created by changes in the stationary wave field with a high-pressure anomaly over East Asia. Local to the change in the stationary wave field and consistent with anticyclonic circulation around a high-pressure cell is a northerly shift in the upper level mean zonal winds. Where zonal winds are enhanced, there is a correlated increase in storm activity that continues over the Arctic and into NE Canada. Similarly, where zonal winds are diminished in the subtropical Pacific, there is a decrease in storm activity that continues across North America and into NE Eurasia.

Precessional forcing of interhemispheric anomalies of poleward moisture transports may also be important to explaining the difference in snowfall rates between NE Canada and NW Eurasia during the month of October. The model simulates increases in moisture transports over the western Pacific that extend northward into the Arctic which is potentially feeding more moisture for snow storms over NE Canada. In contrast, there are equal sized decreases in moisture transports over the eastern Atlantic that may explain part of the decrease in snowfall over NW Eurasia.

In summary, the 2.5 kyr difference in the timing of the maximum in snowfall over NE Canada and NW Eurasia arise from atmospheric processing of precessional forcing within the month of October. The difference in snowfall rates over each of these regions is related to increases in the atmosphere's storm activity over and moisture transports to NE Canada and decreases in storm activity over and moisture transports to NW Eurasia.

10 Discussion

The climate model's response to orbital forcing supports, in part, the Milankovitch hypothesis concerning the importance of reductions in summer insolation on minimizing ablation, and therefore the influence of orbital forcing on glaciation, as can be seen through the 50% variations in positive-degree-days, the proxy measure of potential ablation within the model. What is perhaps less obvious about this confirmation is the fact that potential ablation is not minimized precisely on the summer solstice. Rather, potential ablation is minimized a few weeks earlier, which allows for greater involvement of sea ice and snow feedbacks to influence surface air temperatures. While this small distinction does not produce an appreciable difference in the timing of the minimum in summer insolation with the minimum in potential ablation, the radiative feedbacks are large, upwards of 10 W/m^2 at 115 ka, and indicate that a sizable portion of the modeled variations in potential ablation are an indirect response to orbital forcing. This finding could be important to some aspects of the debate of whether glacial initiation is limited by an inadequate supply of moisture or too much summer ablation. One mechanism that has been proposed to increase the moisture supply to sites of glacial initiation is an active thermohaline circulation (THC) in the North Atlantic Ocean, through its ability to maintain warmer sea surface temperatures, limit sea-ice growth, and allow for greater evaporation from the ocean surface (Ruddiman and McIntyre 1981; Miller and de Vernal 1992). We show that it is possible for snowfall to increase within a cooler higher latitude climate through enhanced storm activity forced by a greater pole-to-equator temperature gradient. Therefore

there may be some competition between these alternate hypotheses over the role of sea ice in promoting the accumulation of terrestrial ice.

Also in contrast to the ablation-centered Milankovitch hypothesis is the potential importance of changes in snowfall that coincide with time intervals of increased land-ice growth. Although the changes in snowfall were only ∽10 to 20% of its long term mean, these changes could be amplified by the large area represented in a typical ice sheet's accumulation zone. In order to better evaluate the relative importance of either ablation or snowfall on ice-sheet growth or decay we would need, at minimum, to prescribe the evolving shape and size of the North American or European ice sheets. It is also important to note that the changes in snowfall arise from both thermal and dynamic factors that would be difficult to represent within more simplified climate models that are usually used to model the long-term evolution of glacial cycles.

While the model design did not predict the response of ocean circulations to orbital forcing directly, the model was able to predict the atmospheric component of the high-latitude freshwater balance (precipitation minus evaporation or $P - E$) which may have some bearing on orbital forcing of the THC. Because the density of surface waters in the North Atlantic is more sensitive to the high-latitude freshwater balance than the thermal properties of the upper ocean, these tendencies could indicate how the THC would be affected by orbital forcing. Our rationale is that all things being equal, annual mean changes in $P - E$ should lead to lower surface salinities in winter when convection occurs. In reality there may be potential contributions from other factors that affect convection, such as winter temperatures or the freshwater from melting sea ice that is exported from the Arctic. The time series of annual mean $P - E$ averaged between 60–90°N is dominated by the effects of obliquity which accounts for 53.7% of the variance ($\mathbf{A}_o$ = –0.011 m/yr) and is maximized when obliquity is low. The effects of precession are small, accounting for only 29.3% of the variance ($\mathbf{A}_p$ = 0.0026 m/yr), and are maximized when perihelion is on June 26th. While proxy records of the THC are subject to many caveats, one reconstruction of the amount of North Atlantic Deep Water (NADW), which is directly affect by overturning rates, shows generally reduced amounts of NADW between 18 to 30 ka, 58–70 ka, 80–85 ka, 105–112 ka, and 130–150 ka (Labeyrie et al. 1999). These time periods have some correspondence to larger than average $P - E$ values within the model which are maximized 25 to 35 ka, 58–82 ka (with a small local minimum around 72 ka), 100–110 ka, 120–125 ka, and 140–155 ka. This correlation may be more coincidental than this comparison may indicate since one also needs to account for how the growth or decay of land ice itself affects the North Atlantic fresh water balance. Simple scaling estimates of the equivalent reduction in freshwater forcing that could account for the dramatic drop in sea level around 115 ka would indicate that ice sheet growth should also be important to NADW formation (Wang and Mysak 2001).

Whether changes to NADW are important to glacial inception at 115 ka is still uncertain. One study by Khodri et al. (2001) found a 2 Sverdrup (10^6 m^3/s) reduction in the THC and the build-up of perennial snow using a coupled atmosphere-ocean model simulation of the climate system's response to Earth's orbital geometry at 115 ka. Khodri et al. (2001) attributed the build-up of perennial snow to the reduction in the THC and its effect on increasing the meridional surface air temperature gradients and poleward moisture fluxes during summer. The atmosphere-mixed layer ocean model used in the orbital forcing experiment presented here was unable to predict perennial snow for any orbital configuration even though the model predicted even larger changes to the meridional surface air temperature gradient over land and the ocean but about a third less summertime poleward moisture fluxes at 115 ka than found by Khodri et al. (2001). The large number of degree-days simulated by the atmosphere-mixed layer ocean model indicates that the model is capable of melting up to 5 to 8 m of snow during the summer melt season. Besides the fact that poleward fluxes of moisture during summer do not usually end up precipitating as snow over ice-free regions of the Arctic, if that moisture did form snow, it is unlikely that poleward moisture fluxes could be large enough to overcome that threshold without significantly reducing summer temperatures. While changes in ocean circulation are probably important to glacial climate evolution at some level, the thermal response of the upper ocean is largely all that is needed to be in approximate agreement with several observational records of the high latitude surface ocean during the last interglacial (∽112 to 128 ka) (Cortijo et al. 1999) and the mid-latitude ocean over the same time interval (Ruddiman and McIntyre, 1981). In particular, interpretations of sediment cores at high latitudes (60° to 70°N) suggest there was approximately 4 °C cooling over this time interval. The zonally averaged modeled SST over the same latitudes cooled by 4.5 °C. Interpretations of sediment cores in the mid-latitudes (41°N, Ruddiman and McIntyre 1981) also show a 4 °C cooling which is comparable to the 3.5 °C cooling that occurs in the model. The Ruddiman and McIntyre data, however, are not consistent with more recently published data from other mid-latitude sediment cores (Cortijo et al. 1999) which indicate the mid-latitudes warmed by 4 °C over this time interval. The finding that the atmosphere-mixed layer ocean model's response to orbital forcing is linear to precessional and obliquity forcing, as seen by the close correspondence between the red curves and model derived time series in Figs. 2, 7, 12, and 14, indicates that many of the findings presented here could have been derived from four equilibrium experiments (in addition to the control): one simulation with eccentricity set to zero and

obliquity at its mean value, one simulation with a 1° increase or decrease in obliquity with eccentricity set to 0, and two simulations with eccentricity set to a reasonable value (say 0.04), obliquity set to its mean value, and two values of the longitude of the perihelion 90° apart. Considering the large amount of variability that is present within these models, each of these separate integrations would need to be very long to reduce the amount of error that is created by including noise as part of the experimentally derived signals (optimally 100 years or more). The linear approximation will be the least representative of the fully nonlinear response within the polar regions. We found annual mean sea-ice thickness to have the most nonlinear response to orbital forcing of any simulated quantity with nonlinearities account for about 33% of the signal. This nonlinearity was also manifest in other quantities affected by sea-ice thickness, but to a lesser degree. For instance, nonlinearities in the response of annual-mean sea-ice concentration 60°N to 90°N accounts for only 9% of the signal. While the non-linear response is not very dominant, its presence in the Arctic regions means it may still be an important element of the connection between orbital forcing and glacial cycles.

11 Conclusions

The equilibrium response to continuous variations in Earth's orbital geometry over the past 165 kyr is derived within an atmospheric general circulation model coupled to a mixed layer ocean and thermodynamic/dynamic model of sea ice. The computational expense of this calculation has been reduced by two means. Firstly, the atmospheric component involves a relatively low-resolution nine-level and approximately 4.5 by 7.5° grid spacing. Secondly, the variations in orbital geometry have been accelerated by a factor of 30 which is consistent with the relatively short equilibration time of the atmosphere-slab ocean system which is on the order of 10 years, or more than three orders of magnitude faster than the most rapidly varying component of orbital forcing. These economies allowed the experiment to be completed within a 5500-model-year integration. The response of the model to orbital forcing is overwhelming linear with the exception of sea-ice thickness. The dominantly linear response permitted the mathematical separation of the effects of precession from the effects of obliquity that greatly enhanced the ability to interpret model predictions in terms of changes in the seasonal and annual mean insolation.

The orbital configuration that was found to be most glaciation-friendly occurs when obliquity is low and aphelion occurs is in late spring through the combined influence a reduced potential-ablation and enhanced snowfall. The climate model simulates prominent minima in potential-ablation at 26, 73, and 117 ka and secondary minima at 97 and 142 ka that coincide within a few thousand years to the maxima and secondary maxima in snowfall. These time intervals correspond to phases of falling sea level and terrestrial ice growth as indicated by the marine $\delta^{18}O$ record.

We track the thermal and dynamical processes affecting potential ablation and snowfall through the influence of orbital forcing on surface air temperature. In particular we noted that obliquity and precession affect the seasonal and annual mean climate within the Arctic similarly, largely because of feedbacks and properties of sea ice. An enhanced meridional temperature gradient during late fall and early winter provided mainly by the response of sea ice but also because of cloud feedbacks at low latitudes and a reduction in the poleward heat transports by stationary waves all contribute to the increase in storm activity that correlates with the time intervals of enhanced snowfall. The exact timing of the maxima in snowfall can be affected by zonal asymmetries in the model climate created in part by the atmosphere stationary wave response to orbital forcing. The fact that orbital forcing leads to increases in snowfall during the same time intervals as when potential ablation is minimized is one of the most significant conclusions of the present modeling exercise. This would imply that the connection between orbital forcing and glacial and interglacial cycles is much more intimately involved in the sometimes complex internal processing of the climate system than might be assumed if the amount of terrestrial ice is primarily a function of local changes in insolation as is often assumed.

Appendix

Energy is transported to the poles in the form of sensible heat, potential energy, latent heat, and kinetic energy. Because poleward transport of kinetic energy is a small fraction of the total transport we do not include it within our calculations. Given monthly means, one may mathematically calculate energy transported by *SE*, the *MMC*, and by all circulations ($Total = SE + MMC + TE$). Because daily information from the model was not saved, we needed to determine *TE* as a residual ($TE = Total - SE - MMC$). This calculation of *TE* is particularly sensitive to small errors which we have minimized by two means. Firstly we saved monthly means of the triple product of surface pressure, meridional wind velocity and each of the quantities pertaining to air temperature, geopotential height, and specific humidity at every model level as well as the covariance of the meridional wind and surface pressure. Neglecting the time variation of surface pressure from this calculation can seriously undermine the fidelity of the calculation. The second way we minimize errors is by adjusting the meridional winds to yield no net exchange of mass across latitudinal circles (i.e., there are no vertically integrated meridional winds, Hall et al. 1994). Although there can be a true mass flux associated with changes in surface pressure, these fluxes are smaller than the errors introduced by not enforcing this constraint (Masuda 1988). We adjust the meridional winds by the monthly mean of the vertical integral of the covariance between meridional winds and surface pressure. The accuracy of the heat transport calculation can be tested by a comparison between the heat transport calculated directly from the appropriate quantities from the model integration and the heat transport as inferred from the radiative imbalance at the top-of-the-atmosphere. The two curves are both quite smooth and never differ by more than 0.1 PW.

References

Berger A (1992) Orbital variations and insolation database (contribution 92-007, NOAA/NGDC, Boulder, USA)

Berger A (1978) Long-term variations of caloric insolation resulting from the Earth's orbital elements. Quat Res 9: 139–167

Blackmon ML (1976) A climatological spectral study of the 500 mb geopotential height of the northern hemisphere. J Atmos Sci 33: 1607–1623

Braithwaite RJ (1995) Positive degree-day factors for ablation on the Greenland ice sheet studied by energy-balance modelling. J Glaciol 41(137): 153–160

Broccoli AJ (2000) Tropical cooling at the Last Glacial Maximum: an atmosphere-mixed layer ocean model simulation. J Clim 13(5): 51–976

Broccoli AJ, Manabe S (1987) The influence of continental ice, atmospheric CO_2, and land albedo on the climate of the last glacial maximum. Clim Dyn 1: 87–99

Cook KH, Held IM (1988) Stationary waves of the ice age climate. J Clim 1: 807–819

Cortijo E, Lehman S, Keigwin L, Chapman M, Paillard D, Labeyrie L (1999) Changes in meridional temperature and salinity gradients in the North Atlantic Ocean (30°–72°N) during the last interglacial period. Paleoceanography 14(1): 23–33

Deblonde G, Peltier WR (1991) Simulations of continental ice sheet growth over the last glacial-interglacial cycle: experiments with a one-level seasonal energy balance model including realistic geography. J Geophys Res 96(D5): 9189–9215

Deblonde G, Peltier WR (1993) Late Pleistocene Ice Age scenarios based on observational evidence. J Clim 6: 709–727

Dong B, Valdes PJ (1995) Sensitivity studies of northern hemisphere glaciation using an atmospheric general circulation model. J Clim 8: 2471–2496

Felzer B, Webb III T, Oglesby JR (1998) The impact of ice sheets, CO_2, and orbital insolation on late Quaternary climates: sensitivity experiments with a general circulation model. Quat Sci Rev 17: 507–534

Flato GM, Hibler WD (1995) Ridging and strength in modeling the thickness distribution of Arctic sea-ice. J Geophys Res 100(C9): 18,611–18,626

Gallee H, van Ypersele JP, Fichefet T, Marsiat I, Tricot C, Berger A (1992) Simulation of the last glacial cycle by a coupled, sectorially averaged climate-ice sheet model 2. Response to insolation and CO_2 variations. J Geophys Res 97(D14): 15, 713–15,740

Gallimore RG, Kutzbach JE (1995) Snow cover and sea ice sensitivity to generic changes in Earth orbital parameters. J Geophys Res 100(D1): 1103–1120

Gallimore RG, Kutzbach JE (1996) Role of orbitally induced changes in tundra area in the onset of glaciation. Nature 381: 503–505

Hall NMJ, Hoskins BJ, Valdes PJ, Senior CA (1994) Storm tracks in a high resolution GCM with doubled carbon dioxide. Q J R Meteorol Soc 120: 1209–1230

Hays JD, Imbrie J, Shackleton NJ (1976) Variations in the Earth's orbit: pacemaker of the ice ages. Science 194: 1121–1132

Held I (1982) Climate models and the astronomical theory of the ice ages. ICARUS 50: 449–461

Imbrie J and coauthors (1984) The orbital theory of Pleistocene climate: support from a revised chronology of the marine d18O record. In: Berger AL, Imbrie J, Hays J, Kukla G, Saltzman B (eds) Milankovitch and climate. D Reidel, Dondrecht, pp 269–305

Imbrie J and coauthors (1992) On the structure and origin of major glaciation cycles 1. linear responses to Milankovitch forcing. Paleoceanography 7(6): 701–738

Imbrie J and coauthors (1993) On the structure and origin of major glaciation cycles. 2. The 100,000-year cycle. Paleoceanography 8(6): 699–733

Joussaume S, Braconnot P (1997) Sensitivity of paleoclimate simulation results to season definitions. J Geophys Res 102(D2): 1943–1956

Joussaume S, Taylor KE (1995) Status of the Paleoclimate Modeling Intercomparison Project (PMIP) In: Gates WL (ed) Proce 1st Int AMIP Scientific Conference. WCRP Report, pp 425–430

Kageyama M, D'Andrea F, Ramstein G, Valdes PJ, Vautard R (1999) Weather regimes in past climate atmospheric general circulation model simulations. Clim Dyn 15(10): 773–793

Khodri M, Leclainche Y, Ramstein G, Braconnot P, Marti O, Cortijo E (2001) Simulating the amplification of orbital forcing by ocean feedbacks in the last glaciation. Nature 410: 570–574

Kutzbach JE (1987) Model simulations of the climatic patterns during the deglaciation of North America. In: The Geology of North America vol K-3, North America and adjacent oceans during the last deglaciation. The Geological Society of America, pp 425–445

Kutzbach JE, Guetter PJ (1986) The influence of changing orbital parameters and surface boundary conditions on climate simulations for the past 18,000 years. J Atmos Sci 43(16): 1726–1759

Labeyrie L, Leclaire H, Waelbroeck C, Cortijo E, Duplessy JC, Vidal L, Elliot M, Le Coat B (1999) Temporal variability of the surface and deep waters of the North West Atlantic Ocean at orbital and millennial scales. In: Clark PU, Webb RS, Keigwin LD (eds) Mechanisms of global climate change at millennial time scales. Geophysical Monograph 112, AGU, Washington DC, pp 77–98

Ledley TS, Chu S (1995) The initiation of ice sheet growth, Milankovitch solar radiation variations, and the 100 ky ice age cycle. Clim Dyn 11: 439–445

Ledley TS, Pfirman S (1997) The impact of sediment-laden snow and sea ice in the arctic on climate. Clim Change 37: 641–664

Lindberg C, Broccoli AJ (1996) Representation of topography in spectral climate models and its effect on simulated precipitation. J Clim 9(11): 2641–2659

Manabe S, Broccoli AJ (1995) The influence of continental ice sheets on the climate of an ice age. J Geophys Res 90: 2167–2190

Manabe S, Stouffer RJ (1980) Sensitivity of a global climate model to an increaseof CO_2 concentration in the atmosphere. J Geophys Res 85(C10): 5529–5554

Marsiat I (1994) Simulation of the Northern Hemisphere continental ice sheets over the last glacial-interglacial cycle: experiments with a latitude-longitude vertically integrated ice sheet model coupled to a zonally averaged climate model. Paleoclimates 1(1): 59–98

Masuda K (1988) Meridional heat transport by the atmosphere and the ocean: analysis of FGGE data. Tellus 40A: 285–302

Milankovitch M (1941) Canon of insolation and the ice age problem (Israel Program for Scientific Translations, Jerusalem)

Miller GH, de Vernal A (1992) Will greenhouse warming lead to Northern Hemisphere ice-sheet growth? Nature 355: 244–246

Mitchell JFB (1993) Modelling of paleoclimates: examples from the recent past. Philos Trans R Soc Lond B 341: 267–275

de Noblet N, Prentice IC, Joussaume S, Texier D, Botta A, Haxeltine A (1996) Possible role of atmosphere–biosphere interactions in triggering the last glaciation. Geophys Res Lett 23(22): 3191–3194

Oglesby RJ (1990) Sensitivity of glaciation to initial snow cover, CO_2, snow albedo, and oceanic roughness in the NCAR GCM. Clim Dyn 4: 219–235

Peltier WR, Marshall S (1995) Coupled energy-balance/ice-sheet model simulations of the glacial cycle: a possible connection between terminations and terrigenous dust. J Geophys Res 100(D7): 14,269–14,289

Phillipps PJ, Held IM (1994) The response to orbital perturbations in an atmospheric model coupled to a slab ocean. J Clim 7: 767–782

Prell WL, Kutzbach JE (1987) Monsoon variability over the past 150,000 years. J Geophys Res 92(D7): 8411–8425

Rind D, Peteet D, Kukla G (1989) Can Milankovitch orbital variations initiate the growth of ice sheets in a general circulation model? J Geophys Res 94: 12,851–12,871

Ruddiman WF, McIntyre A (1981) Oceanic mechanisms for amplification of the 23,000-year ice-volume cycle. Science 212: 617–627

Shackleton NJ (1987) Oxygen isotopes, ice volume and sea level. Quat Sci Rev 6: 183–190

Shackleton NJ (2000) The 100 000-year ice age cycle identified and found to lag temperature, Carbon dioxide and orbital eccentricity. Science 289: 1897–1902

Short DA, Mengel JG, Crowley TJ, Hyde WT, North GR (1991) Filtering of Milankovitch cycles by Earth's geography. Quat Res 35: 157–173

Schneider SH, Thompson SL (1979) Ice ages and orbital variations: some simple theory and modeling. Quat Res 12: 188–203

Suarez M, Held IM (1979) The sensitivity of an energy balance climate model to variations in the orbital parameters. J Geophys Res 84(C8): 4825–4836

Tarasov L, Peltier WR (1997) Terminating the 100 ky ice age cycle. J Geophys Res 102(D18): 21,665–21,693

Vavrus S (1999) The response of the coupled Arctic sea ice-atmosphere system to orbital forcing and ice motion at 6 ky and 115 ky BP. J Clim 12: 873–896

Vettoretti G, Peltier WR (2003a) On Post Eemian glacial inception. Part I: the impact of summer seasonal temperature bias. J Clim 16(6): 889–911

Vettoretti G, Peltier WR (2003b) On Post Eemian glacial inception. Part II: elements of a "cryospheric moisture pump". J Clim 16(6): 912–927

Wang Z, Mysak LA (2001) Ice sheet-thermohaline circulation interactions in a climate model of intermediate complexity, J Oceanography 57: 481–494

Young MA, Bradley RS (1984) Insolation gradients and the paleoclimate record. In: Berger AL, Imbrie J, Hays J, Kukla G, Saltzman B (eds) Milankovitch and climate. D Reidel, Dardrecht, pp 707–713